

A Novel Path to Runaway Electron Mitigation via Deuterium Injection and Current-Driven MHD Instability

C. Paz-Soldan,^{1,2} C. Reux,³ K. Aleynikova,⁴ P. Aleynikov,⁴ V. Bandaru,⁵ M. Beidler,⁶ N. Eidielis,¹ C. Liu,⁷ Y.Q. Liu,¹ A. Lvovskiy,¹ S. Silburn,⁸ L. Bardoczi,¹ L. Baylor,⁶ I. Bykov,^{9,1} D. Carnevale,¹⁰ D. Del-Castillo Negrete,⁶ X. Du,¹ O. Ficker,¹¹ S. Gerasimov,⁸ M. Hoelzl,⁵ E. Hollmann,⁹ S. Jachmich,¹² S. Jardin,⁷ E. Joffrin,³ M. Lehnen,¹² E. Macusova,¹¹ A. Manzanares,¹³ G. Papp,⁵ G. Pautasso,⁵ Z. Popovic,⁹ F. Rimini,⁸ D. Shiraki,⁶ C. Sommariva,¹⁴ D. Spong,⁶ S. Sridhar,³ G. Szepesi,⁸ C. Zhao,⁷ and the DIII-D Team and JET Contributors*¹⁵

¹General Atomics, PO Box 85608, San Diego, CA 92186-5608, United States of America

²Department of Applied Physics and Applied Mathematics, Columbia University, New York, NY 10024, USA^{a)}

³CEA, IRFM, F-13108 Saint Paul Lez Durance, France

⁴Max-Planck-Institut für Plasmaphysik, Teilinstitut Greifswald, D-17491 Greifswald, Germany

⁵Max Planck Institute for Plasma Physics, Boltzmannstr. 2, 85748 Garching b. M., Germany

⁶Oak Ridge National Laboratory, Oak Ridge, TN 37831-6169, TN, United States of America

⁷Princeton Plasma Physics Laboratory, Princeton, NJ 08543, NJ, United States of America

⁸CCFE, Culham Science Centre, Abingdon, Oxon, OX14 3DB, United Kingdom

⁹Center for Energy Research, University of California San Diego - La Jolla, CA 92093-0417, United States of America

¹⁰Dipartimento di Ing. Civile e Ing. Informatica, Università di Roma Tor Vergata, Rome, Italy

¹¹Institute of Plasma Physics of the CAS, Prague, Czech Republic

¹²ITER Organization, Route de Vinon, CS 90 046, 13067 Saint Paul Lez Durance, France

¹³Centro de Investigaciones Energeticas, Medioambientales y Tecnológicas, Madrid, Spain

¹⁴Ecole Polytechnique Fed. de Lausanne (EPFL), Swiss Plasma Center (SPC), Lausanne, Switzerland

¹⁵*See the author list of ‘Overview of JET results for optimising ITER operation’ by J. Mailloux et al to be published in Nuclear Fusion Special issue: Overview and Summary Papers from the 28th Fusion Energy Conference (Nice, France, 10-15 May 2021)

(Dated: 2 June 2021)

Relativistic electron (RE) beams at high current density (low safety factor, q_a) yet very low free-electron density accessed with D_2 secondary injection in the DIII-D and JET tokamak are found to exhibit large-scale MHD instabilities that benignly terminate the RE beam without measurable first-wall heating. This scenario thus offers an unexpected alternate pathway to achieve RE mitigation without collisional dissipation. Benign termination is explained by two synergistic effects. First, during the MHD-driven RE loss events both experiment and MHD orbit-loss modeling supports a significant increase in the wetted area of the RE loss. Second, as previously identified at JET and DIII-D, the fast kink loss timescale precludes RE beam regeneration and the resulting dangerous conversion of magnetic to RE kinetic energy. During the termination the RE kinetic energy is lost to the wall but the current fully transfers to the cold bulk, enabling benign Ohmic dissipation of the magnetic energy on longer timescales via a conventional current quench. Hydrogenic (D_2) secondary injection is found to be the only injected species that enables access to the benign termination. D_2 injection: 1) facilitates access to low q_a in existing devices (via reduced collisionality & resistivity), 2) minimizes the RE avalanche by ‘purging’ the high-Z atoms from the RE beam, 3) drives recombination of the background plasma, reducing the density and Alfvén time, thus accelerating the MHD growth. This phenomenon is found to be accessible when crossing the low q_a stability boundary with rising current, falling toroidal field, or contracting minor radius - the latter being the expected scenario for vertically unstable RE beams in ITER. While unexpected, this path scales favorably to fusion-grade tokamaks and offers a novel RE mitigation scenario in principle accessible with the day-one disruption mitigation system (DMS) of ITER.

I. INTRODUCTION AND MOTIVATION

Relativistic electrons (REs) excited during a tokamak disruption are well recognized as a critical concern to the reliable operation of high-current tokamaks such as ITER¹⁻⁴. While the first line of defense is to achieve dis-

^{a)}Electronic mail: carlos.pazsoldan@columbia.edu

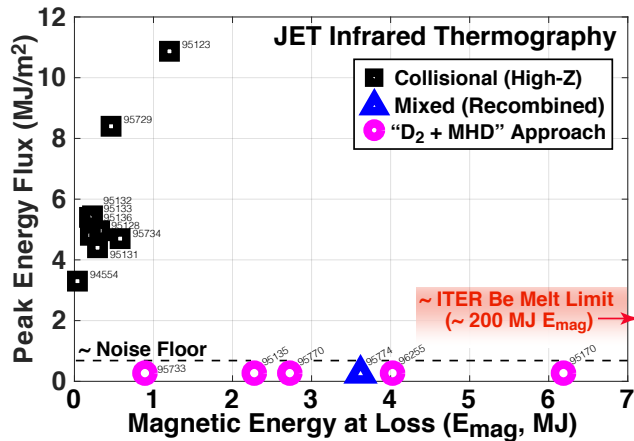


FIG. 1. Peak energy flux measurements in JET from infrared (IR) thermography. An increasing trend of energy flux with I_{RE} is found when using high-Z injection, yet dramatically the energy flux is below the noise floor when D_2 injection is used, despite access to far higher I_{RE} being accessed.

ruption mitigation while avoiding REs in the first place, a second line of defense is needed to minimize the potential for damage from any unavoidable RE populations. This second line of defense is called RE mitigation, and the baseline ITER strategy for this is the injection of massive quantities of high-Z atoms (neon) using shattered pellet injection (SPI)⁵. Injection of high-Z atoms are intended to maximize the collisional dissipation level within the RE beam, and as such reduce the RE current (I_{RE}) as quickly as possible. Unfortunately, the collisional approach is challenged by low rates of high-Z assimilation into the RE beam (slowing collisional damping)^{6–8} as well as the acceleration of the vertical instability^{9,10}. This final effect is predicted to cause the termination of the ITER RE beam on the first wall to occur at the same I_{RE} regardless of the high-Z quantity assimilated^{11,12}. New approaches to the RE mitigation problem are thus needed.

Recent observations on DIII-D¹³ and JET¹⁴ reveal a promising alternate pathway for mature RE beam mitigation by: 1) injecting D_2 to recombine the background plasma, reducing density (n_e) and decreasing the Alfvén time (τ_A), and 2) crossing the low q_a stability boundary^{15–19} with low n_e/τ_A to excite large-scale and fast current-driven MHD instabilities. Strikingly, despite termination in JET of RE currents (I_{RE}) up to 1.5 MA and magnetic energies ($E_{mag} \propto I_{RE}^2$) up to 6 MJ the energy flux to the first-wall is found to be below the thermography noise floor for these “ D_2 +MHD” termination events, as shown in Fig. 1. This figure also shows that these levels of I_{RE} and E_{mag} are well above that which drives significant energy fluxes with the baseline high-Z RE mitigation scheme. These results are favorable for ITER, though its challenge will be greater since 50x more E_{mag} must be managed while only allowing peak heat fluxes a few times greater than the JET ther-

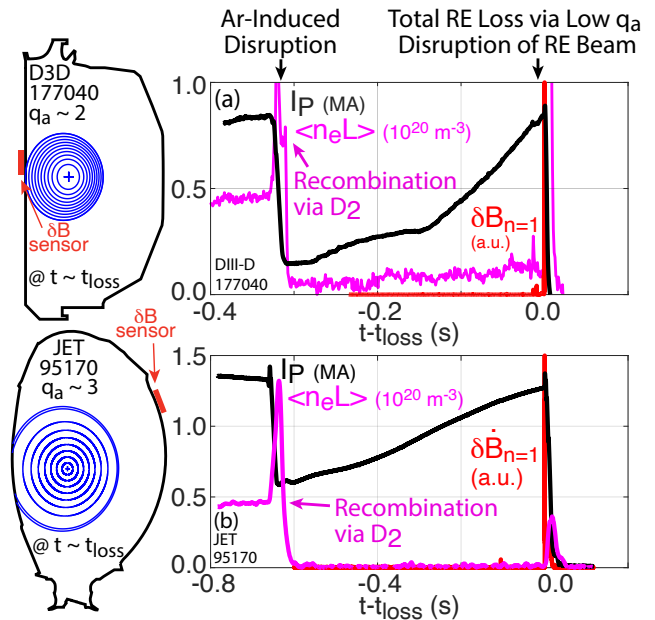


FIG. 2. Observation of “ D_2 +MHD” loss events in DIII-D and JET. Access to relatively low q_a in the presence of a recombined plasma state resulting from D_2 injection promotes large-scale and fast current-driven MHD instabilities that terminate the RE beam in a *second disruption*. These early examples reach low q_a by increasing I_P , but later cases find the same dynamics with contracting minor radius at constant I_P to decrease q_a .

mography noise floor. These discharges demonstrate a novel approach to RE beam mitigation which will be the subject of this work to understand and extrapolate to ITER.

Before describing the detailed phenomenology, Fig. 2 shows the basic features of RE mitigation with the D_2 +MHD approach on DIII-D and JET. The basic features are the same on both devices. First, REs are intentionally created for study using Ar primary injection to trigger the RE-producing disruption. Shortly following the Ar primary injection, a secondary D_2 injection is delivered (via SPI or massive gas injection, MGI) that immediately *recombines* the background plasma²⁰. The recombined background plasma expels the residual Ar impurity²¹ and yields a relatively *collisionless* RE beam state, which can then evolve towards current-driven instability. In these examples, a fixed loop voltage (V_{loop}) combined with the reduced collisionality (resistivity) increases I_{RE} until a current limit (low q_a limit) is reached. A fast and large-scale MHD ($\delta B/B$) instability is accessed, which then effectively causes a *second disruption* of the plasma and drives sudden and complete RE loss to the first-wall. Surprisingly, the large-scale $\delta B/B$ and total loss is in fact found to minimize the wall heating, owing to a larger RE impact wetted area and reduction of kinetic (E_{kin}) to magnetic (E_{mag}) energy conversion as will be described in this work. Although the fast kink has been observed before, most notably during early high

current RE beams during JET limiter operation in the 1980s, only in the discharges described in this study has D₂ injection been applied and the synergy with the collisionless background plasma state identified. Furthermore those early observations did not benefit from the increased modeling capability now available for deployment to understand the foundational mechanisms of this effect.

This contribution will summarize these findings in terms of the basic benign termination phenomenology (Sec. II), discuss MHD modeling of the observed phenomenology (Sec. III), move into discussion of experimental access conditions via databases and controlled scans (Sec. IV), and conclude with an extrapolation of this RE mitigation scheme to ITER (Sec. V). This work expands upon the first discovery of this effect in DIII-D (reported in Ref.¹³) by presenting additional MHD modeling and dedicated experimentation, and further provides additional supporting evidence to the JET data recently reported in Ref.¹⁴.

II. PHENOMENOLOGY OF THE BENIGN TERMINATION

A detailed description of the phenomenology of the MHD event in DIII-D and the subsequent deconfinement of the RE population is given in Ref.¹³. This description is here summarized and supplemented with corresponding IR thermography images. A comparison of a high- I_{RE} , low q_a , recombined loss event is compared to a traditional high q_a , ionized loss event in Fig. 3. As with Fig. 2, low q_a is here accessed by raising I_{RE} , though in later experiments the minor radius a is contracted to access low q_a at constant or decreasing I_{RE} (noting $q_a \propto aB_T/I_P$). Note the interferometer signal ($\langle n_e L \rangle$) reveals the most striking pre-loss indicator of the benign termination: a lack of free-electron density (n_e) indicating a largely recombined background plasma. As presented in Ref.²¹, D₂ causing recombination is understood to arise when the energy loss channel for the input Ohmic power switches from ionization to D₂ neutral conduction. As neutral conduction begins to dominate, the bulk temperature (T_e) is lowered below the threshold for ionization, and the plasma recombines. At that point, the only remaining free electrons are runaways, and the plasma is very collisionless. The residual small resistivity is dominated by RE-neutral D₂ collisions²². The D₂ quantity required to achieve this effect is rather low, and scales with the Ohmic power density²¹.

The dynamics of the RE final loss (at $t=t_{loss}$) are totally different when the plasma is recombined. The recombined case shown exhibits two discrete HXR bursts indicating strong MHD-driven loss (other discharges have only one), evidenced by a very large $\delta B/B$ of almost 5% measured on the high-field side (HFS, as in Fig. 2). The discrete HXR bursts are followed by an absence of HXR emission indicating that all REs have been lost. Subse-

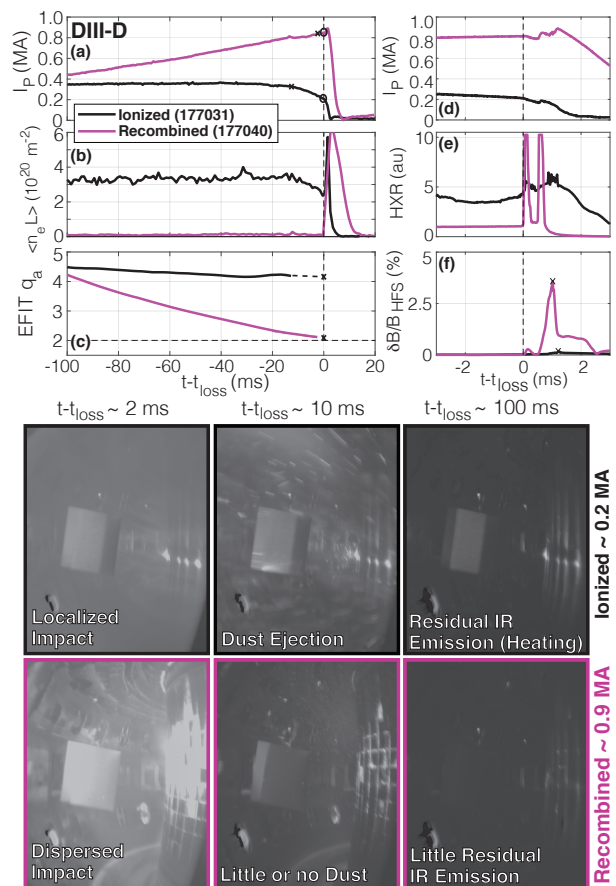


FIG. 3. Comparison of conventional (black) and benign (magenta) RE loss events in DIII-D. The loss event transitions from a gradual process to a singular event with a large $\delta B/B$, a large HXR flash, a large impact wetted area, and an absence of persistent IR emission (heating).

quently, the plasma re-ionizes, indicating a transfer of the RE current back into bulk thermal current. In contrast, the traditional loss event does not have the large-scale $\delta B/B$, does not have similarly pronounced HXR spikes, and the HXRs persists during the current quench (CQ) phase. The presence of HXRs during the current quench (CQ) indicates the transfer of E_{mag} into RE E_{kin} , which is a damaging phenomenon as $E_{mag} \gg E_{kin}$ ^{23–25}.

IR camera data (looking opposite the forward-beamed emission) also included in Fig. 3 illustrates the qualitatively different first-wall impact of these two loss scenarios. In the conventional scenario discussed in detail in Ref.²⁶, a localized RE impact is found (complete with carbon dust ejection), followed by persistent wall IR emission, indicating some localized heating occurred. The large $\delta B/B$ loss scenario, in contrast, has a much larger wetted area as evidenced by the broader impact-induced emission, followed by little or no dust, and little or no persistent IR emission. These images thus support the basic concept that the large-scale $\delta B/B$ loss events spread the RE E_{kin} over a larger wetted area, which will be later revisited in Sec. III.

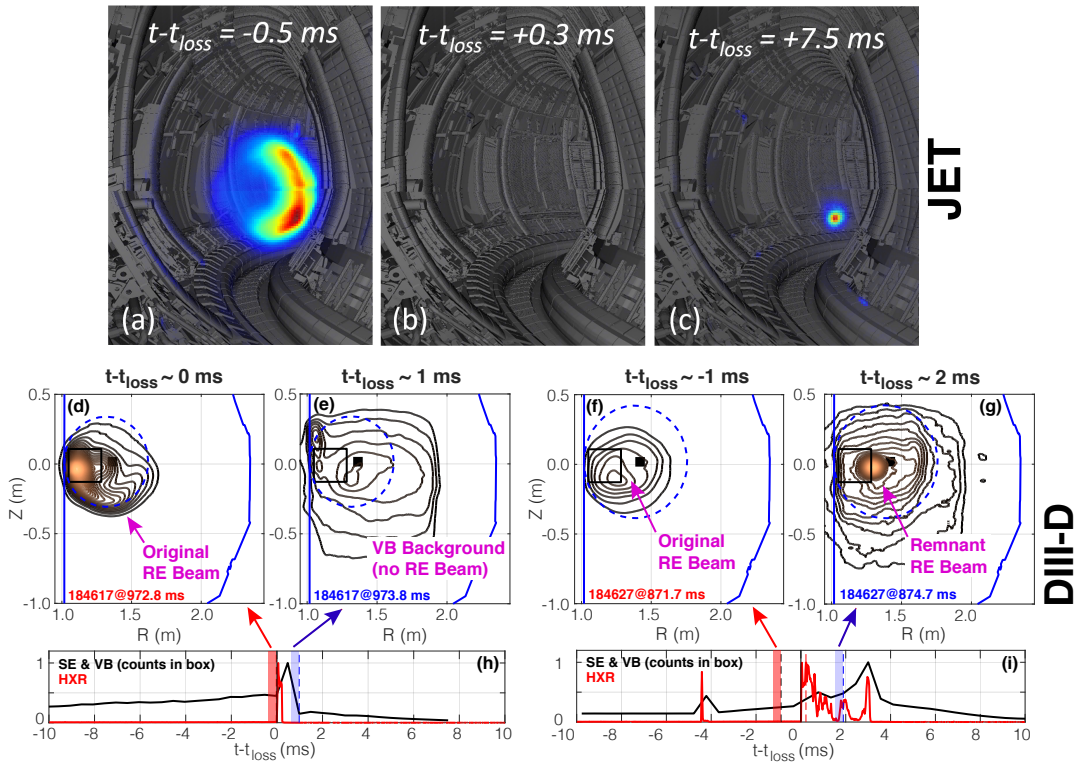


FIG. 4. Synchrotron emission in JET and DIII-D, revealing (a,b,d,e) benign cases with complete deconfinement of the RE beam from large-scale $\delta B/B$ event, or (c,f,g) non-benign cases with only a partial deconfinement and emergence of a remnant beam. The remnant in JET (c) appears due to a maximized secondary avalanche gain, while in DIII-D (f,g) the $\delta B/B$ induced loss is incomplete.

Synchrotron emission (SE) shown in Fig. 4 supports the interpretation that the RE beam can be suddenly and totally eliminated by the large-scale $\delta B/B$. JET and DIII-D SE data both show a transition from a conventional crescent-shaped SE pattern to no emission at all (in the case of JET) or a very weak residual emission (in DIII-D, with the residual due to thermal visible bremsstrahlung emission). This transition occurs over just one camera frame, or under one ms, which is the same time-scale of the fast $\delta B/B$ shown in Fig. 3(f). The SE also reveals the existence of loss events that do not permanently eliminate the REs, with two incomplete loss scenarios identified. In the first incomplete loss scenario, the HXR emission is not fully eliminated prior to the CQ. Persistent HXR during the CQ then indicates transfer of E_{mag} to E_{kin} , as shown in Fig. 4(f)-(g). In a second incomplete loss scenario, a gradual re-emergence of a tiny remnant beam appears ‘out of the noise’, as shown in Fig. 4(b)-(c). This second scenario is observed only in JET with maximized secondary avalanche gain, indicating that a tiny unmeasurable remnant RE population was re-avalanched to a measurable size. The impact of the avalanche gain varying from DIII-D to JET to ITER will be discussed in Sec. V C.

These highlighted discharges are supported by an extended database of JET RE loss events, shown in Fig. 5, covering most RE beam terminations of the JET IWL

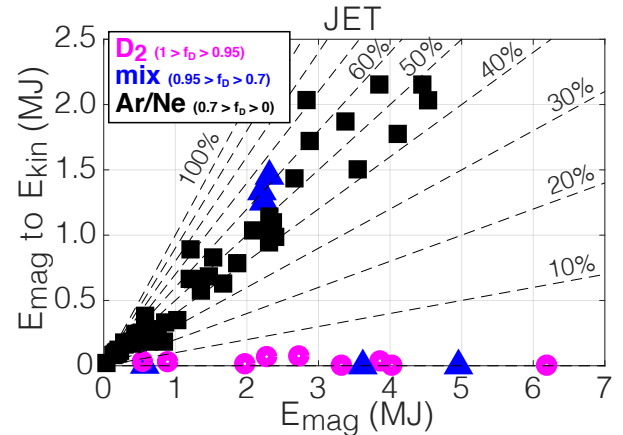


FIG. 5. Calculated conversion of E_{mag} to E_{kin} for JET, with the high D_2 purity (f_D) cases showing very low conversion while the high-Z dominated cases show appreciable conversion. Intermediate mixtures can exhibit both benign and non-benign terminations.

period¹⁴. This database shows that if the D_2 purity (f_D) is sufficiently high (D_2 being $>95\%$ of the injected atoms), no E_{mag} to E_{kin} conversion is computed. Where no conversion is found, the entire RE population is lost and the current promptly converted into thermal bulk Ohmic current. E_{mag} is then benignly dissipated as uniform radiation from the now conventional thermal CQ¹³.

In contrast, as originally reported in Ref.²³, the high-Z cases are computed to convert about half of E_{mag} into E_{kin} , which then further deposits as localized heating (evidenced by Fig. 1)²⁴. This is a very problematic result for high-Z collisional dissipation, as in both JET and ITER $E_{mag} \gg E_{kin}$. Figure 5 also shows that intermediate purity situations can exhibit either outcome, indicating a critical quantity of D₂ is needed. In JET, sufficient D₂ purity is straight forward to achieve by using pure D₂ in the secondary SPI. Experimental access to the benign termination scenario will be discussed in Sec. IV, after first-principles MHD modeling of the benign termination is discussed.

III. MHD MODELING OF THE BENIGN TERMINATION

First-principles MHD modeling captures the essential features of benign termination phenomenology. Extended MHD modeling (JOEKE³⁰ for JET²⁹, M3D-C1³¹ for DIII-D^{27,28}) shown in Fig. 6 demonstrates that the near-total deconfinement of the RE beam and transfer of the RE current into thermal bulk current is well captured by computational approaches that employ a fluid treatment of the RE population. Both simulations find the large $\delta B/B$ drives near-total stochasticity of the plasma, allowing REs to promptly be lost via parallel transport. In both simulations, the prompt loss of REs require via Faraday's law that the current transfer promptly back into bulk current. For this to occur, the loss must occur very rapidly - faster than the secondary avalanche growth can replace the lost REs. This condition is enabled by D₂ injection, which as will be discussed in Sec. IV both accelerates the MHD loss events as well as reduces the secondary avalanche growth rate.

Detailed examination of Fig. 6 reveals that the nature of the underlying MHD instability is potentially different in JET and DIII-D, with a double-tearing mode at $q_a \approx 5$ identified in JET pulse 95135^{14,29}, yet a conventional low q_a (2-3) kink instability found in all DIII-D pulses^{13,32}. Differences in the expected instability likely arise from differences in the shape of the RE current profile, with broader (or hollow) current profiles naturally expected to exhibit current-driven instability at higher q_a than more peaked profiles³³. JET current profiles are inferred to be broader (or hollow), consistent with the observation of MHD excitation at higher q_a to be shown in Sec. IV. These contrasting findings suggest that the total MHD deconfinement and RE-to-bulk current conversion is insensitive to the detailed nature of the MHD instability, so long as $\delta B/B$ grows to sufficient size to deconfine the full RE population and allow the current to transfer to the Ohmic bulk.

Further MHD and RE transport modeling using the MARS-F^{28,32} and KORC³⁴ codes enable elucidation of the necessary levels of $\delta B/B$ to deconfine the full RE population and further allows estimation of the wetted area

over which the RE kinetic energy spreads during these loss events. These calculations are shown for DIII-D in Fig. 7 and for JET in Fig. 8. This modeling is carried out by first using the MARS-F code to compute the linear stability of the RE beam reconstructed equilibrium. For the MHD stability analysis, the equilibrium is taken to consist of only the cold bulk, with the current carried by REs thus ascribed to the bulk plasma. The eigenfunction of the least stable eigenmode is extracted and used as the input δB field in later RE transport calculations with MARS-F and KORC simulations. The magnitude of the eigenfunction is then arbitrarily scaled, until the modeled δB at the location of a magnetic sensor approximately matches the experimental poloidal field sensor measurement. For each δB magnitude, the orbits expected for a spatially uniform RE distribution at a given energy (here 10 MeV) and pitch angle (here small, $\approx 10^\circ$) are calculated, both through the plasma region as well as the vacuum region, until they impact the limiter. Note the scaling of a linear instability eigenmode to an experimental sensor measurement enables significant simplification of the overall problem, but cannot capture non-linear effects in the mode structure nor saturation mechanisms.

Considering DIII-D in Fig. 7, MARS-F modeling supports a progressively larger fraction of RE loss as $\delta B/B$ is increased. At experimentally relevant levels ($\delta B/B \approx 5\%$), nearly all RE orbits are lost. The experimental loss fraction ($\approx 100\%$) is greater than the simulation, likely due to the longer interaction time (100s μs) than simulated. These calculations are also for single specific energy and pitch angle. REs populate a wide distribution of energy and pitch, so calculations should consider the expected distribution function to arrive at a more accurate prediction of the fractional RE loss. MARS-F modeling predicts an increased wetted area when the RE beam is deconfined by large-scale $\delta B/B$ for DIII-D, consistent with Fig. 3. Further evidence for the large wetted area from spatially distributed HXR sensors in DIII-D is found in Ref.¹³.

Considering JET in Fig. 8, both MARS-F and KORC simulations have been carried out. KORC uses as input the same scaled eigenfunction calculated by MARS-F linear stability analysis, but it includes a full-orbit treatment of the RE orbit³⁴ while MARS-F uses a guiding center approach³⁵. This difference also requires a different initialization of the pitch angle, with a constant magnetic moment used to populate the MARS-F calculations. Nonetheless, both MARS-F and KORC produce comparable RE loss fractions, and near total RE loss is again predicted. Both MARS-F and KORC also recover the increased wetted area as $\delta B/B$ is increased. For this JET discharge note the experimental $\delta B/B$ is in excess of 1%, though the large distance from the δB sensor to the plasma (denoted d) places a large uncertainty on the $\delta B/B$ inside the plasma, since the Eigenmode is found in MARS-F to fall off like $\delta B \propto d^{-3}$.

Finally, it is worth noting that the problem of predict-

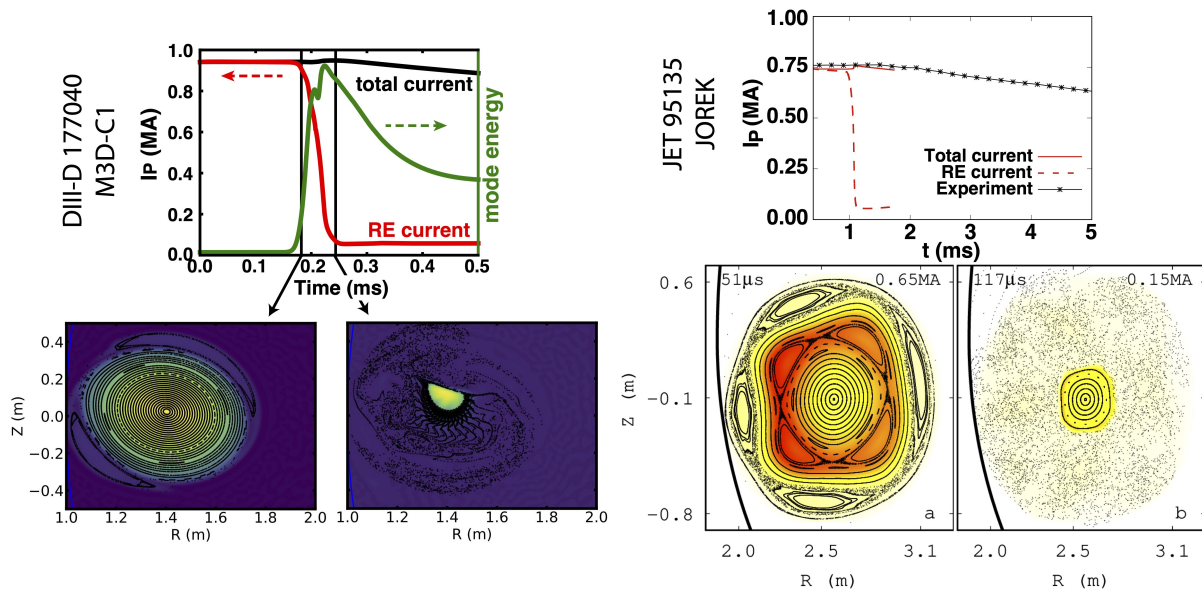


FIG. 6. Non-linear extended MHD modeling with a RE fluid model (M3D-C1 for DIII-D^{27,28}, JOREK for JET²⁹) demonstrate conversion of RE to bulk current after a large-scale MHD event. The DIII-D instability computed is a conventional $q_a=2$ resistive external kink, while the JET instability computed is a double-tearing mode due to the input hollow current profile.

ing the RE wetted area under the conventional high-Z dissipation approach is unsolved, with ad-hoc estimates used in assessments of RE impact for ITER^{36,37}. A notable feature of the D_2 +MHD approach is that it enables direct computation of the RE wetted area expected for the various RE orbits. Furthermore, by convolving the orbits with the expected RE distribution function and using non-linear extended MHD simulation to predict the $\delta B/B$, a fully first-principles prediction of the first-wall wetted area and energy loading from RE terminations should be possible. The implications of these computed wetted areas for dispersing E_{kin} of RE beams in ITER will be discussed in Sec. V.

IV. EXPERIMENTAL CONDITIONS TO ACCESS THE BENIGN TERMINATION

Attention now turns to the experimental conditions required to access the benign termination scenario, as access is not guaranteed simply by injecting D_2 . First, ensemble databases of DIII-D and JET will be used to explore the role of I_P , q_a , and $\delta B/B$. This database will reveal the additional importance of a recombined (low n_e) state in both devices, enabled by hydrogenic (D_2) injection. Next, controlled scans in DIII-D and JET will be used to reinforce the database findings. These scans explore the role of background plasma composition, current profile broadness, and the vertical instability.

A. Database Analysis

DIII-D and JET database data demonstrating the experimental factors correlated with the benign termination are shown in Fig. 9. The DIII-D database also includes a collection of non-RE ‘regular’ plasma matched disruptions. Consideration is first given to low safety factor access (q_a) in Fig. 9(a,b). Low q_a access is found to be facilitated by D_2 injection (in that it is statistically more likely) but significant variation exists. That is, cases without D_2 also can also reach low q_a ^{24,38}, and D_2 cases can also (rarely) undergo a loss event at intermediate q_a ($\approx 4-5$). The preponderance of D_2 loss events in both JET and DIII-D however occur at conventionally low q_a (2-3 in DIII-D, 3 in JET). The expectation from first principles is that the current profile broadness governs the critical q_a for large-scale instability^{33,39}, though it is difficult to measure the broadness for these near-circular RE beams⁴⁰.

Next, the magnitude of δB is shown as a heatmap against q_a and I_P in Fig. 9(c,d). Note that as discussed in Sec. III, a steep radial fall-off is expected, with $\delta B \propto d^{-3}$, where d is the distance from the magnetic axis to the δB sensor. Nonetheless, we see that in DIII-D a clear trend of increasing $\delta B/B$ is found both as q_a is lowered and I_P rises. Interestingly, the thermal reference cases (without REs) are also in-line with this trend, indicating the $\delta B/B$ accessed may not be directly influenced by the RE population. The situation in JET is found to be much less clear along these axes, with a wide variance of δB observed even at low q_a and high I_P . The reason for this is unclear, but may be due to either sensitivities in the radial δB fall-off, or a wider variety of current profile shapes found in JET (ex, both hollow and peaked pro-

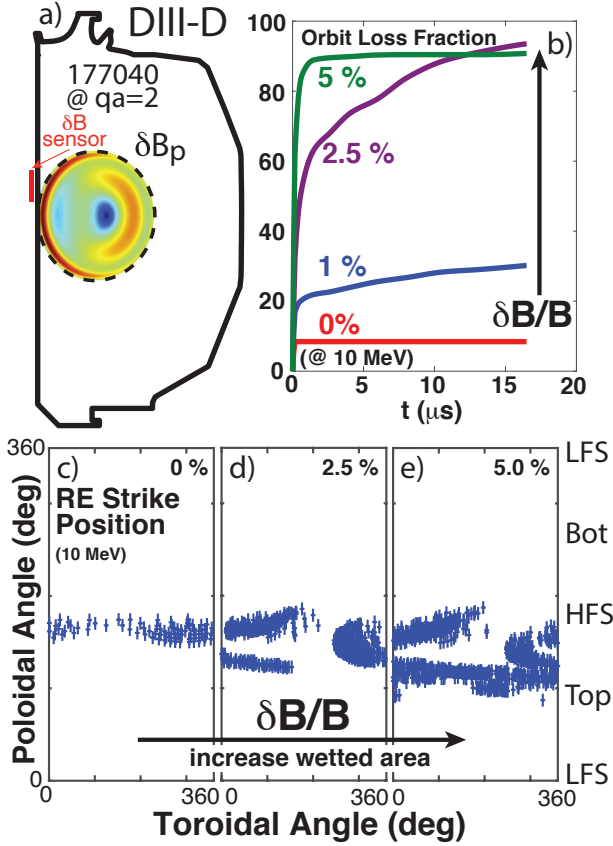


FIG. 7. MARS-F RE-orbit modeling of the RE orbit loss in DIII-D. Increasing $\delta B/B$ magnitude drives a progressively larger fraction of RE orbits to be lost, and these orbits impact the limiting surface with a progressively larger wetted area. Experimental δB measured on the HFS sensor is 1 kG, thus $\delta B/B \approx 5\%$.

files) as compared to DIII-D (only peaked profiles). The current profile effect will be discussed in Sec. IV C.

Finally, a pseudo-growth rate of the instability ($d(\delta B/B)/dt$) is compared. This metric is extracted by taking the linear growth rate of the $\delta B/B$ signal, and has the natural unit of %/ms, since $\delta B/B$ grows by several % in less than one ms (see Fig. 3[f]). Here, the findings are clear and consistent for both DIII-D and JET. D_2 cases in both exhibit a markedly faster $d(\delta B/B)/dt$, which is especially true if the plasma is fully recombined (low $\langle n_e L \rangle$). This is consistent with an Alfvénic growth, with the fully recombined nature of the equilibrium (low n_e) enabling a particularly fast MHD growth (short τ_A). For sufficiently high B_T and low n_e , the Alfvén velocity can approach the speed of light, indicating the usual MHD frequency ordering is no longer appropriate. Previous theoretical work indeed predicted a progressively faster MHD instability growth rate for RE beams as the Alfvén velocity approached the speed of light⁴¹. Particularly interesting in this paradigm are the DIII-D non-RE reference discharges, which access high $\delta B/B$ but not high $d(\delta B/B)/dt$, again supporting the key role of re-

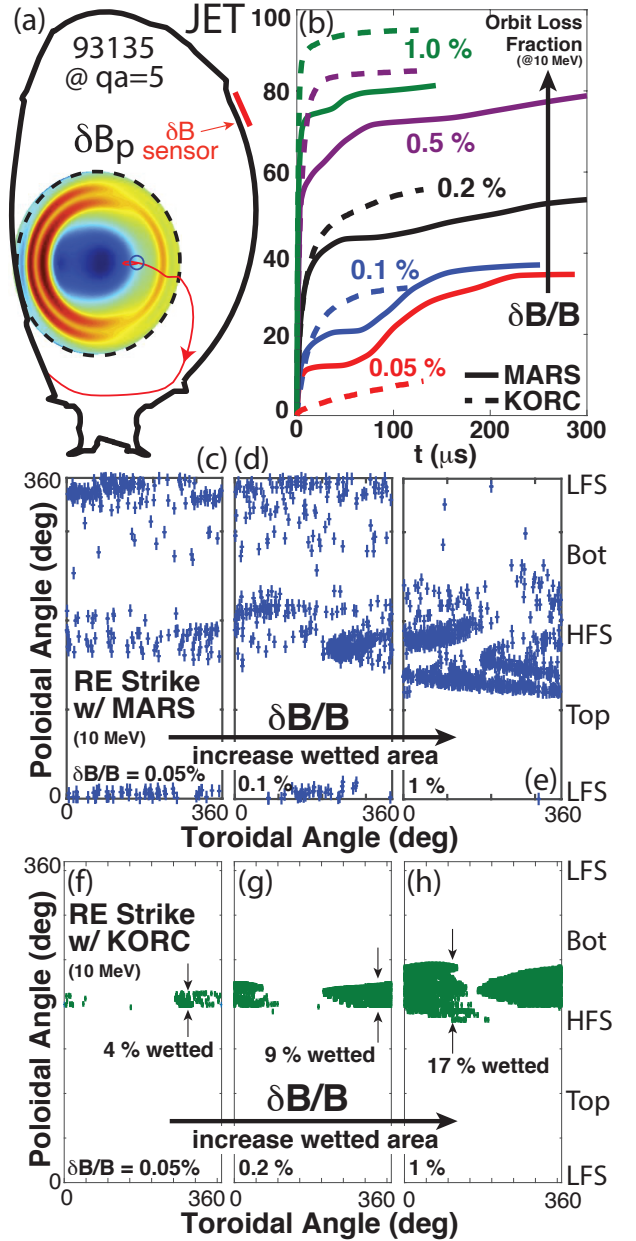


FIG. 8. MARS-F and KORC modeling of the RE orbit loss for JET. Increasing $\delta B/B$ drives a larger fraction of RE orbit loss with progressively larger wetted areas. Experimental values for JET is 7G on the distant sensor, mapping to over 1% $\delta B/B$ on the plasma surface (with large uncertainty due to the large distance from the plasma to the magnetic sensor).

ducing τ_A .

To conclude, experimental access to the benign termination in DIII-D and JET is facilitated by: 1) a recombined plasma state (enabled by D_2 injection), 2) access to low q_a (more likely with D_2 injection), and 3) high current (facilitated by D_2 injection in existing devices). These findings will now be reinforced with controlled scans.

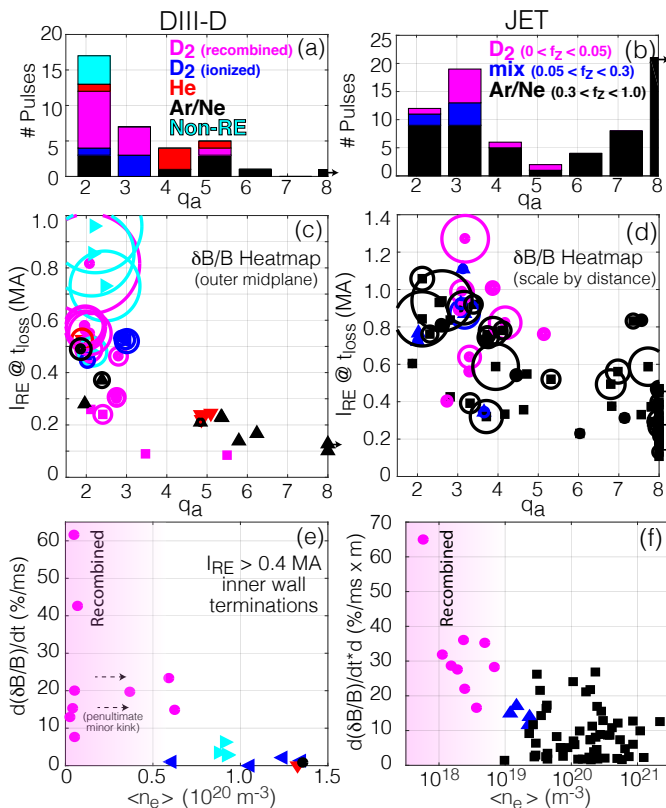


FIG. 9. Database comparison of RE loss events for both DIII-D and JET, demonstrating access to low q_a , magnitude of observed $\delta B/B$ and $d(\delta B/B)/dt$ as a function of I_P , q_a , and $\langle n_e L \rangle$.

B. Background Bulk Plasma Composition

Variations of the background plasma composition in DIII-D and JET reveal the importance of high D_2 purity and potential access limits for too little or too much D_2 injection. Figure 10 (left) presents a controlled scan of the background composition from D_2 , He, Ar, and non-RE reference ‘regular’ plasma (few keV bulk temperature). These plasmas are compressed onto the centerpost to reduce a and q_a at roughly constant I_P and B_T , recalling $q_a \propto aB_T/I_P$. q_a is extracted from standard EFIT reconstructions⁴². Matched cases are selected which terminate at approximately the same I_P and q_a , to highlight the species effect. Both the D_2 RE beam and the non-RE plasma access the large $\delta B/B$ and disrupt with a conventional I_P -spike. Interestingly, despite He being considered low-Z, the He dynamics are instead identical to the high-Z cases shown in Fig. 3 and are not benign, supporting the role of the recombined background plasma as opposed to the ion species directly. The conventional high-Z dissipation case also as expected does not excite a large $\delta B/B$. Interestingly, the non-RE references, while having the same $\delta B/B$, have a much slower $d(\delta B/B)/dt$.

Exploring the role of the secondary D_2 injection quantity in Fig. 10(right), both a qualitative lower and upper limit to the requisite D_2 quantity is observed in DIII-

D. That is, with too little or too much D_2 , it is possible to not access the benign termination. This result is somewhat troubling, but the limiting phenomena are fairly clear and so may be amenable to first-principles extrapolation. Considering the lower limit, the limiting phenomenon is a lack of recombination. The required quantities to avoid this outcome depend on the Ohmic input power and can be estimated for existing devices as well as ITER from the model presented in Fig. 21. The limiting phenomena at too high a D_2 quantity is an inhibited access to low q_a . What occurs instead is the development of minor MHD instabilities at higher q_a that lose the recombined state without ever accessing the large $\delta B/B$. Interestingly, examination of Fig. 10(g) shows a rise in V_{loop} ahead of the appearance of the minor instability. As such, the hypothesis is that the increased dissipation from the higher D_2 quantity (via RE-neutral D_2 collisions²²) begets a transition back to the high-Z like loss scenario, though the mechanism for this is not yet understood. Indeed, the high-Z termination scenario itself is poorly understood. In JET, D_2 is delivered from the SPI system⁵ and within its injection quantity limits neither a lower nor an upper bound in D_2 injection quantity is observed. Overall, the high- D_2 quantity limit is highlighted as an important area to understand the extrapolation of this approach.

While experiments in JET did not find an impact of the D_2 quantity within the explored range, a scan in primary injection Ar quantity did impact the termination dynamics as described in Ref. 14 and is shown in Fig. 11. This scan actuates the D_2 purity by varying the Ar quantity at constant D_2 secondary injection quantity. All purity levels are found to lead to bulk plasma recombination and all access the benign termination. However, as the Ar quantity is increased the radiated power during the current quench (CQ) is increased, and consequently the CQ rate and induced electric field is also increased. The higher electric field combined with the presence of more bound electron targets increases the computed secondary avalanche gain^{43,44}, as will be quantified in Sec. V C. At the highest Ar quantity, the increased avalanche gain leads to the re-emergence of a tiny (but measurable) remnant RE beam after the benign termination, as pictured in Fig. 4(c). This indicates that the RE loss induced by the large $\delta B/B$ was not total - and that the secondary amplification of the remnant can occur. These findings motivate further consideration of the impact of the avalanche gain to the benign termination in ITER as will be discussed in Sec. V C.

C. Equilibrium Access Paths to Current-Driven Instability

Attention now turns to equilibrium access to the large $\delta B/B$ instability, and the impact of crossing the low q_a instability boundary with variable I_P , B_T , and a dynamics in DIII-D, noting $q_a \propto aB_T/I_P$. These scans are motivated by the fact that the early discovery of this ef-

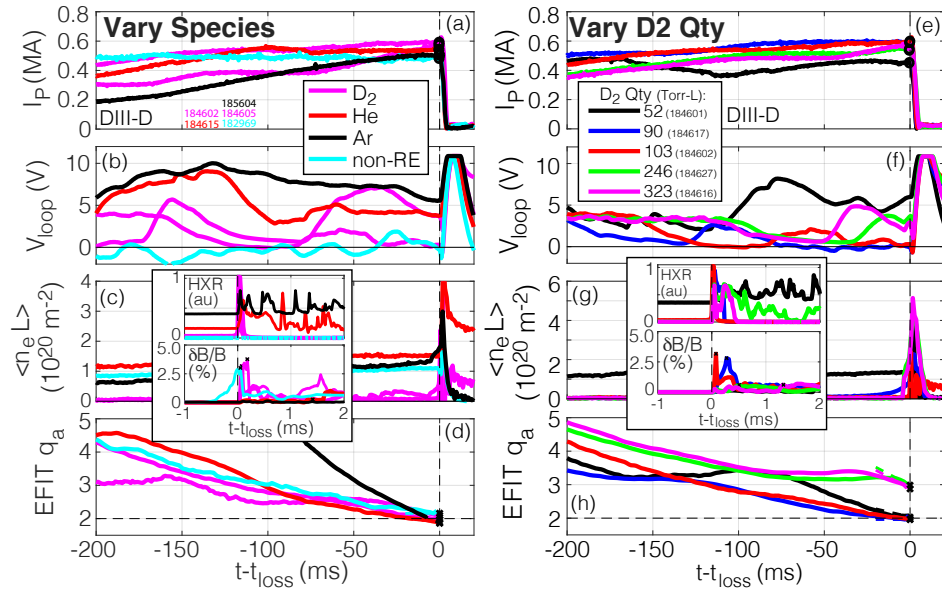


FIG. 10. Controlled scans varying (left) the background plasma composition in DIII-D reveal that D₂ is uniquely able to access the large and fast $\delta B/B$ in the RE beam. (right) Varying the D₂ quantity reveals limits at too low (no recombination) and too high (impeded low q_a access) D₂ quantity.

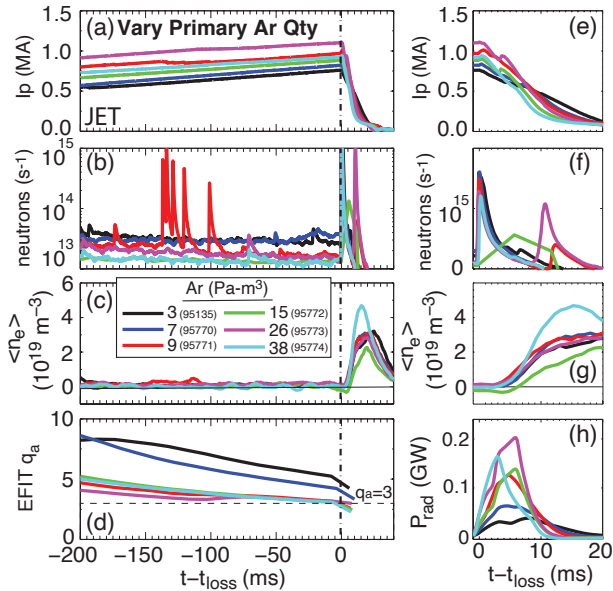


FIG. 11. Varying the quantity of Ar injected to trigger the RE-producing disruption in JET modifies the dynamics after the benign termination is initiated. Increased radiation and accelerated CQ at higher Ar quantity allows the re-appearance of a tiny but measurable remnant RE beam, also pictured in Fig. 4(c).

fect was done with rising I_P and fixed a , as shown in Fig. 2¹³. Conversely, as will be discussed in Sec. V A, ITER vertically unstable post-disruption RE beams are expected to access low q_a with falling I_P but contracting a . Note the fixed I_P falling a path was also used in Fig. 10, but with vertically controlled position.

Dedicated scans in DIII-D shown in Fig. 12 access the

benign termination with variable rates of change of I_P (left), B_T (center), and a (right), all of which vary q_a . Considering I_P rate of change, Fig. 12(left) shows that the benign termination can be accessed with both increasing, constant, and slightly decreasing I_P . Where I_P is constant, a contraction is used to reduce q_a . Note all cases remained recombined, and so when q_a reached 2 the benign termination immediately took place. Considering the resultant $\delta B/B$, there may be a slightly increase in $\delta B/B$ with rising I_P , but all cases reach very large $\delta B/B$ values near 5%. As such, the rising I_P of the early cases shown in Fig. 2 is not considered to be an essential requirement though it may be a favorable effect. Rising I_P should also broaden the current profile, owing to the finite time needed for an applied V_{loop} to penetrate to the RE beam core.

Variations of B_T shown in Fig. 12(center) are also pursued to examine the role of current profile broadness, enabled by the fact that falling B_T is a significant source of off-axis current drive via induction⁴⁵. All cases again remain recombined. Allowing B_T to fall is clearly found to access the benign termination at higher q_a (≈ 3) than otherwise in DIII-D. Interestingly, the detailed $\delta B/B$ trajectory exhibits a two-spike loss with 1 ms delayed main $\delta B/B$ spike (see inset). Regardless, this finding supports the role of a broad q -profile as enabling access to the benign termination at higher q_a and supports the hypothesis that JET current profiles are systematically broader than DIII-D ones, thus shifting the final loss q_a distribution higher in JET (as seen in Fig. 9).

Finally, the impact of the vertical displacement event (VDE) is explored together with changing background plasma species in Fig. 12(right). With VDE-induced contracting a the D₂ cases are found to access lower q_a

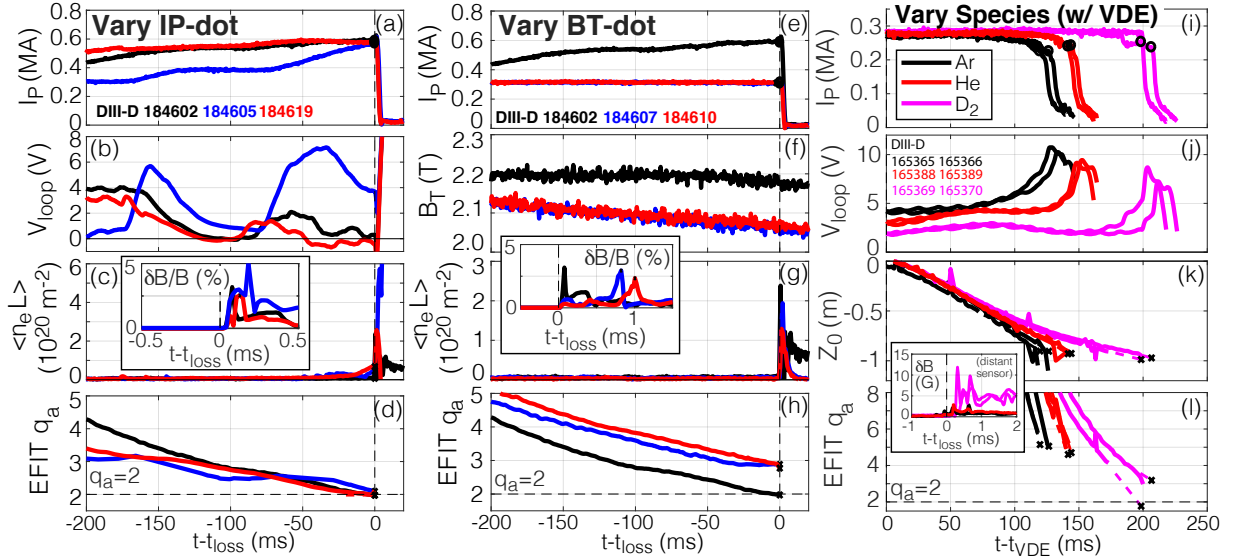


FIG. 12. Access to the low q_a instability ($\propto aB_T/I_P$) is compared when varying the rates of change of I_P vs. a (left), B_T vs. I_P (center), and a during VDE with variable species (right).

before the final loss instability is triggered. This behavior is reminiscent of the high D_2 quantity limit shown in Fig. 10(right). Also worth noting is that the VDE is found to be compatible with access to the benign termination, so long as the other conditions are met. As such, maintenance of a recombined and collisionless plasma is again highlighted as an apparent necessary ingredient to promote access to low q_a during the VDE and eventual excitation of the large-scale $\delta B/B$ instability required to enable the benign termination. The underlying reason may be related to the behavior of conventional ‘hot VDEs’ which due to their collisionless nature compress faster than they can dissipate their current⁴⁶.

V. EXTRAPOLATING THE BENIGN TERMINATION TO ITER

The novel D_2 +MHD RE mitigation path described in this work has been demonstrated to be reproducible in DIII-D and JET, and found in JET to result in minimal energy loading onto the first wall¹⁴. Extrapolation of these findings to ITER requires separate consideration of: 1) ITER’s expected vertically unstable equilibrium evolution; 2) the kinetic energy loading (the large-scale $\delta B/B$ dispersion effect, as shown in Figs. 7-8); and 3) the conversion of magnetic to kinetic energy (ie, Fig. 5) including the role of secondary generation (avalanche) after the second disruption. These topics are now treated in turn.

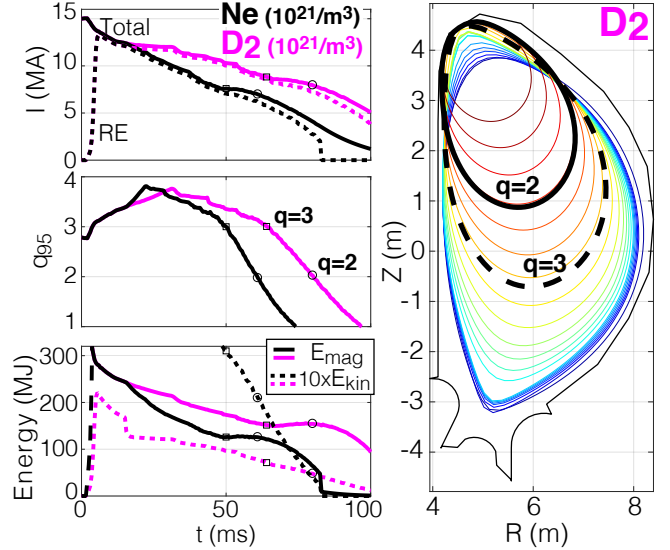


FIG. 13. DINA simulations of an ITER post-disruption CQ with a RE plateau, indicating predicted crossing of $q=3$ and 2. Early evolution is set by area contraction during the VDE, as opposed to collisional dissipation of the RE beam. The trajectory is relatively insensitive to the D_2 quantity.

A. Equilibrium Evolution with Vertical Displacement Event

The equilibrium evolution expected in ITER post-disruption RE beams is dominated by the expected loss of vertical control and resultant VDE. If the ITER plasma is not moved to the neutral point prior to the CQ, only 1 MA of I_P drop will cause a loss of vertical control⁴⁷. If the ITER plasma is moved to the neutral point (pos-

sible if one second advance warning is provided), then a larger I_P drop of 5 MA can be permitted if the CQ rate is slower than 0.5 MA/s⁴⁷.

Focusing on the more dangerous VDE situation, simulations by the DINA code⁴⁸ shown in Fig. 13 find that low q_a (≤ 3) rationals are crossed during the ITER disruption for both D₂ and high-Z (Ne) injection. Indeed, as discussed in Ref.⁴⁹, a wide variety of initial RE seed profiles and magnitudes resulted in fairly similar equilibrium evolutions, indicating this is a robust consequence of the VDE in ITER. DINA simulations find $q_a = 3$ crossing happens due to VDE-driven cross-sectional area contraction with relatively little loss of I_{RE} . As such, around 200 MJ of E_{mag} and a several MJ of E_{kin} must be mitigated. If the $q_a = 3$ crossing does not drive instability, a short while later $q_a = 2$ is crossed, where instability is effectively guaranteed. While these results appear fairly robust, it should be acknowledged that the impact of the VDE growth rate and initial I_{RE} on the mitigation method described herein are important open questions. If initial I_{RE} is very low (q_a very high), significant area contraction would be needed to access sufficiently low q_a . If the VDE growth rate is low, other effects may similarly preclude access to low q_a and large-scale $\delta B/B$. These questions merit further dedicated study in existing devices.

If the ITER plasma remains in vertical control after the CQ, the RE beam may be trivially controlled via slow Ohmic rampdown (ie, solenoid reversal). Considering this possibility, a clear benefit of the D₂+MHD path is that since the excitation of the large-scale MHD is driven by VDE-induced area contraction, a controlled rampdown should naturally avoid the final loss instability. Indeed, the injection of D₂ should slow down the CQ and thus improve the prospects for conventional control. However, for the rest of this discussion, the VDE scenario will be assumed.

B. Kinetic Energy Management via Large Wetted Area

While E_{kin} in ITER is far smaller than E_{mag} , it is still a concern due to the commonly observed highly-localized nature of RE strike energy deposition^{36,50}. As such, dispersal of even just E_{kin} requires a large wetted area enabled by the large $\delta B/B$ of the excited instability⁵¹. Figure 14 presents a comparison of experimentally derived limits to the observed wetted area (as a % of the first-wall), calculated wetted areas from the MARS-F⁵² and KORC³⁴ codes, and ITER expectation of required wetted area to avoid first-wall (Beryllium) melting for an example 5 MJ E_{kin} in ITER.

The DIII-D upper-bound experimental estimate in Fig. 14 is taken by assuming the IR flash pattern in Fig. 3 is toroidally symmetric. The JET lower-bound estimate is taken by converting the IR noise floor of Fig. 1 (0.5 MJ/m²) and scaling it to a minimum wetted area to avoid detection for an estimated E_{kin} of 0.5 MJ in JET (surface

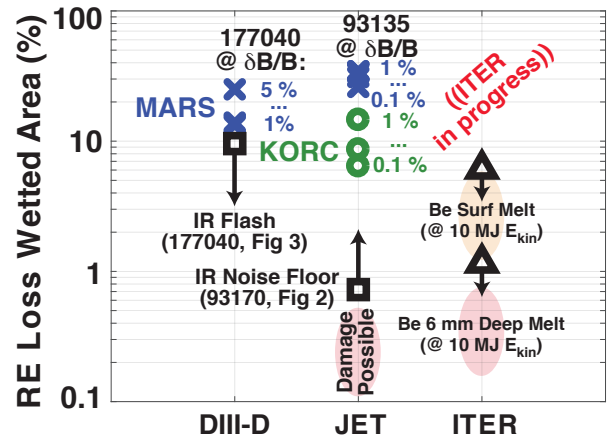


FIG. 14. Comparison of RE loss wetted area from: experimental constraints (squares), MARS-F modeling (\times), KORC modeling (\circ), and approximate ITER blanket module melt limits. **ITER CALCULATIONS IN PROGRESS**

area ≈ 150 m²). It is noteworthy that this yields a requirement for an exceedingly localized RE strike to cause visible heating from E_{kin} alone, and further supports the importance of avoiding conversion of the far larger E_{mag} to E_{kin} (described in the next section). ITER estimates of tolerable wetted area are made by taking the per-module blanket energy limits (0.33 MJ for surface melt, 1.75 MJ for 6 mm deep melt) and scaling to an example RE E_{kin} of 10 MJ. While traditionally quoted ITER E_{kin} is more like 20-30 MJ^{25,53}, D₂ injection also directly reduces the expected E_{kin} as compared to high-Z mitigation. This is because: 1) the collisional dissipation and thus the coulomb logarithm is reduced, mostly via fewer bound electrons, and 2) the expulsion of the high-Z impurity reduces the average RE pitch angle (via reduced pitch-angle scattering) and thus allows the same current to be carried by fewer REs. However, these benefits are compensated somewhat by the higher I_{RE} without collisional dissipation. While detailed calculations should be done, for this study an estimate of 10 MJ is taken which is roughly in line with the above considerations, also shown in Fig. 13(c).

Owing to the expectation that a single large-scale MHD event dominates the entire RE loss, it is possible to defensibly predict the RE wetted area from first principles by simply following orbits to the first wall. These predictions were first shown in Figs. 7 and 8 and are here summarized in Fig. 14 for DIII-D, JET, and ITER. As can be seen, the MARS-F and KORC calculations are rather favorable and consistent across devices. The consistency is not surprising given the self-similar nature of the device geometry and MHD instability across the progression from mid to reactor scale. As such, the excitation of the large-scale $\delta B/B$ appears quite positive for E_{kin} dispersal across devices. A key open question is whether the large-scale $\delta B/B$ will be realized, and how large it will be. This question motivated the scans in Sec. IV. Additional predictive value can be extracted from MHD modeling from JOREK and M3D-C1, which are capable of predicting the non-linearly saturated $\delta B/B$.

This challenging work is underway, and will be validated against data from existing devices.

C. Magnetic Energy Management via Reduced Conversion to Kinetic Energy

Mitigation of the large E_{mag} in ITER is the most severe challenge for RE mitigation. Indeed, the best-case scenario where E_{mag} is dissipated uniformly to the entire first-wall via radiation (100% wetted area) during the CQ is still a significant energy load to the ITER blanket modules⁵⁴. Worse, the conversion of E_{mag} to E_{kin} (with $E_{mag} \gg E_{kin}$) commonly results in localized loading, and so is recognized as a key concern^{23,24}. Figure 5 showed the very favorable result of no conversion from E_{mag} to E_{kin} in JET for D₂ benign terminations¹⁴, a finding that was also reported in DIII-D¹³. This is a consequence of: 1) the large-scale $\delta B/B$ promptly deconfining essentially all REs, and 2) the relatively small avalanche gain factor (n_{RE}/n_{seed}) of these devices. While the self-similarity of MHD provides a basis to expect that the large-scale $\delta B/B$ will still expel essentially all REs in ITER, the avalanche gain effect will be completely different from DIII-D and JET to ITER. Consequently, the amplification of any tiny residual RE population after the RE loss (effectively the new seed) will exponentially increase across these devices.

The changing landscape of the avalanche gain is shown in Fig. 15, where the gain factor is plotted as a function of injection quantity (high-Z and D₂/H₂, noting ITER plans to use Ne and H₂ as opposed to Ar and D₂). The beneficial effect of the high-Z ‘purge’^{20,21} driven by the D₂ injection is clear in both DIII-D and JET, where the Ar expulsion results in a significantly lower expected avalanche gain. Indeed, dedicated scans of the Ar quantity in JET discussed in Sec. IV B revealed the re-emergence of a tiny RE beam (pictured in Fig. 4[c]) at the highest Ar quantities and thus the highest avalanche gain factors accessed in JET. This indicates that the fractional RE loss due to the large-scale $\delta B/B$ may be insufficiently complete, though the possible impact of the higher Ar fraction on the MHD loss dynamics itself complicates this picture. Considering ITER, as is well appreciated the much larger RE current allows a dramatically enhanced avalanche gain. Furthermore, the high-Z expulsion is less beneficial to the expected gain in ITER, at least if the H₂ pellet is fully assimilated. If the H₂ pellet is only fractionally assimilated, a significant drop in avalanche gain is predicted, but the final gain would still be very high compared to if the H₂ pellet were fully assimilated. As such, a large avalanche gain in ITER is nearly impossible to avoid.

Based on the expectation of a large avalanche gain in ITER, the most likely scenario appears to be that the large-scale $\delta B/B$ results in a tiny but finite remnant RE population. This tiny remnant then becomes the seed for a re-avalanched lower current RE beam post-MHD loss,

akin to the higher Ar concentration points in the JET dedicated scan described in Sec. IV B. While possibly dangerous, it is important to note that so long as each time E_{kin} is dispersed with large wetted area and the remnant RE is small, the entire process could in principle be safely repeated a few times. Each loss event would shed a fraction of the initial RE current, resulting in progressively lower E_{mag} and avalanche gain. The key difference then is that the normally localized and continuous RE loss is replaced by a few discrete loss events each with large wetted area. Each discrete event would then result in the minimum level of E_{mag} to E_{kin} conversion. This scheme is pictured graphically in Fig. 16.

A key question for extrapolation to ITER is consequently whether the benign termination can be accessed multiple discrete times within a single post-disruption evolution, or whether the second loss event would be non-benign (like the high-Z cases). Based on the expectation that a recombined state is required to access the large $\delta B/B$, it may be further required to inject additional H₂ pellets after each loss event. This is because the transfer of the RE current into the bulk will drive ionization of the background plasma, at least until the RE beam re-avalanches towards carrying the full current. If the high-Z impurities remain expelled, the recombination may happen naturally. Regardless, injection of multiple H₂ pellets either via a pre-programmed train or asynchronous triggering on the final loss MHD instability is technically feasible with the multi-barrel SPI system presently planned as the day-one ITER DMS. Various elements and open questions of this scheme can be tested in present-day tokamaks and also during the ITER pre-fusion power operation phase.

VI. CONCLUSION AND SUMMARY

Observations on DIII-D and JET reveal a novel benign RE mitigation scenario that has been proven to result in unmeasurable wall heating despite very high values of I_{RE} and E_{mag} . While further experimentation and modeling is needed, these results open an unexpected alternate pathway for RE mitigation in ITER: inject D₂/H₂ and promote the excitation of large-scale MHD by crossing the low q_a stability boundary while in the recombined background plasma state enabled by the D₂/H₂ injection. Recombination is understood to occur via an increase in the neutral conduction of the Ohmic input power, resulting in the temperature falling until ionization can no longer be maintained²¹. Excitation of the large-scale MHD is found to be promoted by D₂ injection, and the largest and fastest $\delta B/B$ is found when the background plasma is recombined while crossing the stability boundary, consistent with previous theoretical work⁴¹. Experimental access to the large-scale $\delta B/B$ is found when crossing the low q_a ($\propto aB_T/I_P$) stability boundary by all paths: increasing I_P , decreasing B_T , or decreasing a , both in vertically stable and unstable situations - so

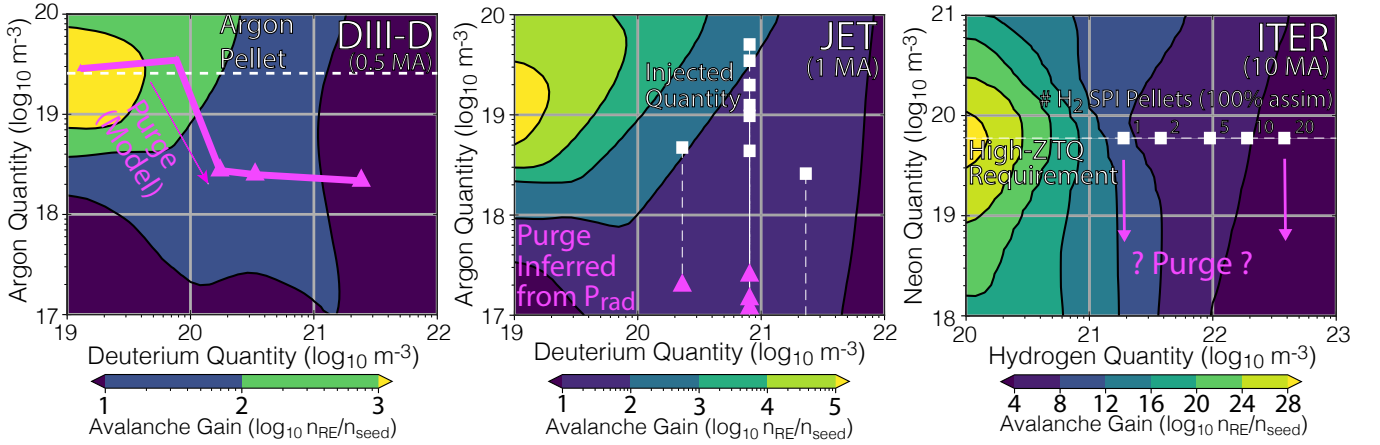


FIG. 15. Expected secondary avalanche gain (n_{RE}/n_{seed}) as a function of impurity density for DIII-D, JET, and ITER. For DIII-D, the experimentally injected n_D is shown along with the computed n_{Ar} from modeling²¹. For JET, the experimentally injected n_D is shown along with the n_{Ar} inferred from radiated power magnitude¹⁴. For ITER, n_H for each SPI pellet is shown.

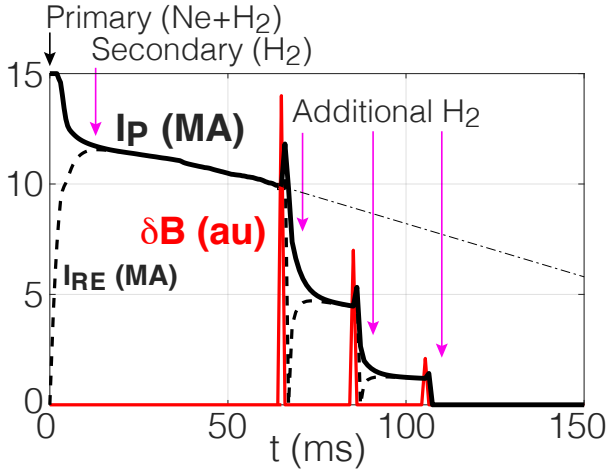


FIG. 16. Cartoon scheme of ITER DMS actuation to exploit the D_2 +MHD RE mitigation path. The large avalanche gain in ITER will likely require a few cycles of the D_2 +MHD loss events. Note ITER plans to use H_2 in place of D_2 in the DMS.

long as the plasma remains recombined. The large-scale MHD is found in experiment and modeling to greatly increase the RE wetted area, providing a favorable pathway to disperse the RE E_{kin} without localized melting. If the MHD is large enough, the large-scale $\delta B/B$ deconfines the RE population with a non-measurable remnant RE population, precluding E_{mag} to E_{kin} conversion in present devices. Extended MHD modeling confirms the prompt transfer of the entire RE current into Ohmic bulk current found in existing devices. Extrapolation of this novel RE mitigation scheme to ITER requires accounting for the much larger avalanche gain expected, which could drive re-avalanche of even a tiny remnant RE population post-MHD. However, if the initial loss is benign, the scheme can in principle be repeated a few times until the total current can no longer re-avalanche any remnant RE population. Validating the repeatability of access to the “ D_2 +MHD” path in situations with high D_2 purity

yet large avalanche gain is thus highlighted as a key validation step that cannot be accessed on present-day tokamaks and awaits pre-fusion power operation in ITER.

VII. ACKNOWLEDGMENTS

Work supported by the US DOE under DE-FC02-04ER54698, DE-SC0020299 and by the ITER Organization (TA C18TD38FU) and carried out within the framework of the EUROfusion Consortium, receiving funding from the Euratom research and training programme 2014-2018 and 2019-2020 under grant agreement No 633053. DIII-D data shown in this paper can be obtained in digital format by following the links at https://fusion.gat.com/global/D3D_DMP. This work was also supported in part by the Swiss National Science Foundation.

VIII. DISCLAIMER

This report was prepared as an account of work sponsored by an agency of the United States Government. Neither the United States Government nor any agency thereof, nor any of their employees, makes any warranty, express or implied, or assumes any legal liability or responsibility for the accuracy, completeness, or usefulness of any information, apparatus, product, or process disclosed, or represents that its use would not infringe privately owned rights. Reference herein to any specific commercial product, process, or service by trade name, trademark, manufacturer, or otherwise, does not necessarily constitute or imply its endorsement, recommendation, or favoring by the United States Government or any agency thereof. The views and opinions of authors expressed herein do not necessarily state or reflect those of the United States Government or any agency thereof. The views and opinions expressed herein do not necessarily reflect those of the ITER

Organization. The views and opinions expressed herein do not necessarily reflect those of the European Commission.

- ¹Hender T C, Wesley J C, Bialek J M, Bondeson A, Boozer A H, Buttery R J, Garofalo A M, Goodman T P, Granetz R S, Gribov Y, Gruber O, Gryaznevich M P, Giruzzi G, Günter S, Hayashi N, Helander P, Hegna C C, Howell D F, Humphreys D A, Huijsmans G T A, Hyatt A W, Isayama A, Jardin S, Kawano Y, Kellman A G, Kessel C E, Koslowski H R, LaHaye R J, Lazzaro E, Liu Y Q, Lukash V, Manickam J, Medvedev S, Mertens V, Mirnov S V, Nakamura Y, Navratil G A, Okabayashi M, Ozeki T, Paccagnella R, Pautasso G, Porcelli F, Pustovitov V D, Riccardo V, Sato M, Sauter O, Schaffer M J, Shimada M, Sonato P, Strait E J, Sugihara M, Takechi M, Turnbull A D, Westerhof E, Whyte D G, Yoshino R, Zohm H, Group, the Itpa Mhd D and Magnet 2007 *Nuclear Fusion* **47** S128–S202 ISSN 0029-5515 URL <https://doi.org/10.1088/0029-5515/47/6/S03>
- ²Lehnen M, Aleynikova K, Aleynikov P B, Campbell D J, Drewelow P, Eidietis N W, Gasparyan Y, Granetz R S, Gribov Y, Hartmann N, Hollmann E M, Izzo V A, Jachmich S, Kim S H, Kočan M, Koslowski H R, Kovalenko D, Kruezi U, Loarte A, Maruyama S, Matthews G F, Parks P B, Pautasso G, Pitts R A, Reux C, Riccardo V, Rocella R, Snipes J A, Thornton A J and de Vries P C 2015 *Journal of Nuclear Materials* **463** 39–48 ISSN 00223115 URL <https://doi.org/10.1016/j.jnucmat.2014.10.075>
- ³Hollmann E M, Aleynikov P B, Fülöp T, Humphreys D A, Izzo V A, Lehnen M, Lukash V E, Papp G, Pautasso G, Saint-Laurent F and Snipes J A 2015 *Physics of Plasmas* **22** 021802 ISSN 1070-664X URL <http://dx.doi.org/10.1063/1.4901251>
- ⁴Boozer A H 2015 *Physics of Plasmas* **22** 032504 ISSN 10897674 URL <http://dx.doi.org/10.1063/1.4913582>
- ⁵Baylor L R, Meitner S J, Gebhart T E, Caughman J B, Herfindal J L, Shiraki D and Youchison D L 2019 *Nuclear Fusion* **59** ISSN 17414326
- ⁶Reux C 2017 Physics of the interaction between runaway electrons and the background plasma of the current quench in tokamak disruptions *Bulletin of the American Physical Society* p N13.3 URL <https://ui.adsabs.harvard.edu/abs/2017APS..DPPNI3003R/abstract>
- ⁷Hollmann E M, Parks P B, Shiraki D, Alexander N, Eidietis N W, Lasnier C J and Moyer R A 2019 *Physical Review Letters* **122** 65001 ISSN 10797114 URL <https://doi.org/10.1103/PhysRevLett.122.065001>
- ⁸Paz-Soldan C, Eidietis N W, Hollmann E M, Aleynikov P B, Carbajal L, Heidbrink W W, Hoppe M, Liu C, Lvovskiy A, Shiraki D, Spong D A, Brennan D P, Cooper C M, Del-Castillo-Negrete D, Du X D, Embréus O, Fulop T, Herfindal J, Moyer R A, Parks P B and Thome K E 2019 *Nuclear Fusion* **59** 066025 ISSN 0029-5515 URL <https://doi.org/10.1088/1741-4326/ab1769>
- ⁹Kiramov D I and Breizman B N 2017 *Physics of Plasmas* **24** 100702 ISSN 1070-664X URL <http://dx.doi.org/10.1063/1.4993071>
- ¹⁰Kiramov D I and Breizman B N 2018 *Physics of Plasmas* **25** 092501 ISSN 10897674 URL <https://doi.org/10.1063/1.5046517>
- ¹¹Konovalov S V 2016 Assessment of the runaway electron energy dissipation in ITER *Proc. of 26th IAEA Fusion Energy Conf. (Kyoto, Japan)* pp TH/7–1 URL <https://conferences.iaea.org/indico/event/98/contributions/11966/>
- ¹²Martin-Solis J R 2020 Formation and termination of runaway beams during vertical displacement events in ITER disruptions *Proc. of 28th IAEA Fusion Energy Conf. (Nice, France)* (Nice, France: IAEA) URL <https://conferences.iaea.org/event/214/contributions/17686/>
- ¹³Paz-Soldan C, Eidietis N W, Liu Y Q, Shiraki D, Boozer A H, Hollmann E M, Kim C C and Lvovskiy A 2019 *Plasma Physics and Controlled Fusion* **61** 054001 URL <https://doi.org/10.1088/1361-6587/aafd15>
- ¹⁴Reux C, Paz-Soldan C and Aleynikov P B 2021 *Physical Review Letters* **126** 175001 URL <https://doi.org/10.1103/PhysRevLett.126.175001>
- ¹⁵Freidberg J P 2014 *Ideal Magnetohydrodynamics* 1st ed (Cambridge University Press) ISBN 978-1107006256
- ¹⁶Wesson J A 1987 *Tokamaks* 1st ed (Oxford: Oxford University Press) ISBN 0198563280
- ¹⁷Bateman G 1978 *Magnetohydrodynamic Instabilities* 1st ed (Boston, Massachusetts: The MIT Press) ISBN 0262021315
- ¹⁸Piovesan P, Hanson J M, Martin P A, Navratil G A, Turco F, Bialek J M, Ferraro N M, R, La Haye R J, Lanctot M J, Okabayashi M, Paz-Soldan C, Strait E J, Turnbull A D, Zanca P, Baruzzo M, Bolzonella T, Hyatt A W, Jackson G L, Marrelli L, Piron L and Shiraki D 2014 *Physical Review Letters* **113** 45003 URL <https://doi.org/10.1103/PhysRevLett.113.045003>
- ¹⁹Turnbull A D, Ferraro N M, Hanson J M, Piovesan P and Martin P A 2016 *Journal of Plasma Physics* **83** 515820301
- ²⁰Shiraki D, Commaux N, Baylor L R, Cooper C M, Eidietis N W, Hollmann E M, Paz-Soldan C, Combs S K and Meitner S J 2018 *Nuclear Fusion* **58** 056006 URL <https://doi.org/10.1088/1741-4326/aab0d6>
- ²¹Hollmann E M, Bykov I, Eidietis N W, Herfindal J L, Lvovskiy A, Moyer R A, Parks P B, Paz-Soldan C, Pigarov A Y, Rudakov D L, Shiraki D and Watkins J G 2020 *Physics of Plasmas* **27** 042515 URL <https://doi.org/10.1063/5.0003299>
- ²²Lvovskiy A, Paz-Soldan C, Eidietis N W, Aleynikov P B, Austin M E, Dal Molin A, Liu Y Q, Moyer R A, Nocente M, Shiraki D, Giacomelli L, Heidbrink W W, Hollmann E M, Rigamonti D, Spong D A and Tardocchi M 2020 *Nuclear Fusion* **60** 056008 URL <https://doi.org/10.1088/1741-4326/ab78c7>
- ²³Loarte A, Riccardo V, Martin-Solis J R, Paley J, Huber A, Lehnen M and Contributors J E 2011 *Nuclear Fusion* **51** 73004 URL <https://doi.org/10.1088/0029-5515/51/7/073004>
- ²⁴Reux C, Plyusnin V V, Alper B, Alves D, Bazylev B and Belonohy E 2015 *Nuclear Fusion* **55** 093013 URL <https://doi.org/10.1088/0029-5515/55/9/093013>
- ²⁵Martin-Solis J R, Loarte A and Lehnen M 2015 *Physics of Plasmas* **22** 082503 ISSN 1070-664X URL <http://doi.org/10.1063/1.4927773>
- ²⁶Hollmann E M, Commaux N, Eidietis N W, Lasnier C J, Rudakov D L, Shiraki D, Cooper C M, Martin-Solis J R, Parks P B and Paz-Soldan C 2017 *Physics of Plasmas* **24** 062505 ISSN 1070-664X URL <http://dx.doi.org/10.1063/1.4985086>
- ²⁷Zhao C, Liu C, Jardin S and Ferraro N M 2020 *Nuclear Fusion* **60** ISSN 17414326 URL <https://doi.org/10.1088/1741-4326/ab96f4>
- ²⁸Liu C, Zhao C, Jardin S, Bhattacharjee A and Brennan D P 2020 *Physics of Plasmas* **27** 092507 URL <https://doi.org/10.1063/5.0018559>
- ²⁹Bandaru V, Hoelzl M, Reux C, Ficker O, Silburn S, Lehnen M, Eidietis N and Team J 2021 *Plasma Physics and Controlled Fusion* **63** 035024 ISSN 0741-3335 URL <https://doi.org/10.1088/1361-6587/abdbcf>
- ³⁰Hoelzl M, Huijsmans G, Pamela S, Becoulet M, Nardon E, Artola F J, Nkonga B, Atanasiu C, Bandaru V, Bhole A, Bonfiglio D, Cathey A, Czarny O, Dvornova A, Feher T, Fil A, Franck E, Futatani S, Gruca M, Guillard H, Haverkort J W, Holod I, Hu D, Kim S, Korving S Q, Kos L, Krebs I, Kripner L, Latu G, Liu F, Merkel P, Meshcheriakov D, Mitterauer V, Mochalskyy S, Morales J, Nies R, Nikulsin N, Orain F, Penko D, Pratt J, Ramasamy R, Ramet P, Reux C, Särkimäki K, Schwarz N, Singh Verma P, Smith S F, Sommariva C, Strumberger E, van Vugt D, Verbeek M, Westerhof E, Wieschollek F and Zielinski J 2021 *Nuclear Fusion* 1–10 ISSN 0029-5515 URL <https://iopscience.iop.org/article/10.1088/1741-4326/abf99f>
- ³¹Jardin S C, Breslau J and Ferraro N 2007 *Journal of Computational Physics* **226** 2146–2174 ISSN 10902716 URL <https://doi.org/10.1016/j.jcp.2007.07.003>
- ³²Liu Y Q, Parks P B, Paz-Soldan C, Kim C C and Lao L L 2019 *Nuclear Fusion* **59** 126021 ISSN 0029-5515 URL <https://doi.org/10.1088/1361-6587/aaf15>

- [//doi.org/10.1088/1741-4326/ab3f87](https://doi.org/10.1088/1741-4326/ab3f87)
- ³³Wesson J A 1978 *Nuclear Fusion* **18** 87–132 ISSN 17414326 URL <https://doi.org/10.1088/0029-5515/18/1/010>
- ³⁴Carbajal L, Del-Castillo-Negrete D, Spong D A, Seal S and Baylor L R 2017 *Physics of Plasmas* **24** 042512 ISSN 1070-664X URL <http://dx.doi.org/10.1063/1.4981209>
- ³⁵Liu Y Q, Paz-Soldan C, Macusova E, Markovic T, Ficker O, Parks P B, Kim C C and Li L 2020 *Physics of Plasmas* **27** 102507 URL <https://doi.org/10.1063/5.0021154>
- ³⁶Lehnen M, Abdullaev S, Arnoux G, Bozhenkov S, Jakubowski M, Jaspers R, Plyusnin V, Riccardo V and Samm U 2009 *Journal of Nuclear Materials* **390-391** 740–746 ISSN 00223115 URL <https://doi.org/10.1016/j.jnucmat.2009.01.200>
- ³⁷Putvinski S V, Baylor L R, Campbell D J, Chuyanov V A, Gribov Y, Leonov V M, Loarte A, Maruyama S, Pearce R, Pitts R A, Polevoi A R and Mitteau R 2010 Disruption Mitigation in ITER Proc. of 23rd IAEA Fusion Energy Conf. (Daejeon, S. Korea) ed IAEA (Daejeon, S. Korea: IAEA) pp ITR/1–6
- ³⁸Hollmann E M, Eidietis N W, Herfindal J, Parks P B, Pigarov A Y, Shiraki D, Austin M E, Bardoczi L, Baylor L R, Bykov I, Carlstrom T N, Kaplan D, Lasnier C J, Lvovskiy A, Moser A, Moyer R A, Paz-Soldan C, Rudakov D L, Samuell C, Shafer M W, Van Zeeland M A, Welander A S and Wilcox R S 2019 *Nuclear Fusion* **59** 106014 ISSN 0029-5515 URL <https://doi.org/10.1088/1741-4326/ab32b2>
- ³⁹Cheng C Z, Furth H P and Boozer A H 1987 *Plasma Physics and Controlled Fusion* **29** 351–366 ISSN 07413335
- ⁴⁰Lao L L, John H S, Stambaugh R D and Pfeiffer W 1985 *Nuclear Fusion* **25** 1421–1436 ISSN 0029-5515 URL <https://doi.org/10.1088/0029-5515/25/10/004>
- ⁴¹Spong D A, Eldridge O C and Kammash T 1977 *Plasma Physics* **19** 817–838 ISSN 00321028 URL <https://doi.org/10.1088/0032-1028/19/9/003>
- ⁴²Lao L L, John H E S, Peng Q and Ferron J R 2005 *Fusion Science and Technology* **48** 968–977 URL <https://doi.org/10.13182/FST48-968>
- ⁴³Zhogolev V E and Kononov S V 2014 *VANT series Nuclear Fusion* **37** 71 URL <https://doi.org/10.21517/0202-3822-2014-37-3-71-88>
- ⁴⁴Hesslow L, Embréus O, Stahl A, Dubois T C, Papp G, Newton S L and Fülöp T 2017 *Physical Review Letters* **118** 1–5 ISSN 10797114 (Preprint 1705.08638) URL <https://doi.org/10.1103/PhysRevLett.118.255001>
- ⁴⁵Garofalo A M, Doyle E J, Ferron J R, Greenfield C M, Groebner R J, Hyatt A W, Jackson G L, Jayakumar R J, Kinsey J E, La Haye R J, McKee G R, Murakami M, Okabayashi M, Osborne T H, Petty C C, Politzer P A, Reimerdes H, Scoville J T, Solomon W M, St John H E, Strait E J, Turnbull A D, Wade M R and VanZeeland M A 2006 *Physics of Plasmas* **13** 056110 ISSN 1070-664X URL <http://doi.org/10.1063/1.2185010>
- ⁴⁶Artola F J, Lackner K, Huijsmans G T, Hoelzl M, Nardon E and Loarte A 2020 *Physics of Plasmas* **27** 032501 ISSN 10897674 URL <https://doi.org/10.1063/1.5140230>
- ⁴⁷Lukash V E, Kavin A A, Gribov Y, Khayrutdinov R R and Loarte A 2013 *40th EPS Conference on Plasma Physics, EPS 2013* **2** 1486–1489 URL <http://ocs.ciemat.es/EPS2013PAP/pdf/P5.167.pdf>
- ⁴⁸Khayrutdinov R R and Lukash V E 1993 *Journal of Computational Physics* **109** 193–201 URL <https://doi.org/10.1006/jcph.1993.1211>
- ⁴⁹Aleynikova K, Huijsmans G T A and Aleynikov P B 2016 *Plasma Physics Reports* **42** 486–494 ISSN 1063-780X URL <http://link.springer.com/10.1134/S1063780X16050019>
- ⁵⁰Reux C, Plyusnin V V, Alper B, Alves D, Bazylev B, Belonohy E, Brezinsek S, Decker J, Devaux S, De Vries P, Fil A, Gerasimov S, Lupelli I, Jachmich S, Khilkevitch E M, Kiptily V G, Koslowski R, Kruezi U, Lehnen M, Manzanares A, Mlyná J, Nardon E, Nilsson E, Riccardo V, Saint-Laurent F, Shevelev A E and Sozzi C 2015 *Journal of Nuclear Materials* **463** 143–149 ISSN 00223115 URL <https://doi.org/10.1016/j.jnucmat.2014.10.002>
- ⁵¹Martin-Solis J R, Loarte A, Hollmann E M, Esposito B and Riccardo V 2014 *Nuclear Fusion* **54** 083027 ISSN 17414326 URL <https://doi.org/10.1088/0029-5515/54/8/083027>
- ⁵²Liu Y Q, Bondeson a, Fransson C M, Lennartson B and Breitholtz C 2000 *Physics of Plasmas* **7** 3681 ISSN 1070664X URL <http://link.aip.org/link/PHPAEN/v7/i9/p3681/s1{&}Agg=doi>
- ⁵³Martin-Solis J R, Loarte A and Lehnen M 2015 *Physics of Plasmas* **22** 092512 ISSN 1070-664X URL <http://dx.doi.org/10.1063/1.4931166>
- ⁵⁴Raffray A R, Calcagno B, Chappuis P, Fu Z, Furmanek A, Jiming C, Kim D H, Khomiakov S, Labusov A, Martin A, Merola M, Mitteau R, Sadakov S, Ulrickson M and Zacchia F 2014 *Nuclear Fusion* **54** 033004 ISSN 00295515 URL <https://doi.org/10.1088/0029-5515/54/3/033004>